FED-Vol. 176, Bubble Noise and Cavitation Erosion
in Fluid Systems
ASME 1993

CAVITATION EROSION POWER AS A SCALING FACTOR FOR CAVITATION EROSION OF HYDRAULIC MACHINES

M. Farhat, F. Pereira, and François Avellan
IMHEF – Institute de Machines Hydrauliques
et de Mécanique des Fluides
EPFL – Swiss Federal Institute of Technology
Lausanne, Switzerland

ABSTRACT

The Cavitation Erosion Power based on the assumption that severe erosion is often due to the repeated collapse of the traveling vortex generated by a leading edge cavity has been formerly introduced. We have shown that cavitation erosion intensity may be scaled by a simple set of flow parameters depending on the mean upstream velocity U, the Strouhal number St corresponding to the main cavity fluctuations, the cavity length l and the pressure in the cavity closure. Further tests have been done to validate this model. In this work we present the results of synchronous pressure fluctuations measurements downstream a leading edge cavity, cavitation induced vibrations and main cavity dimensions. These results show that the pressure fluctuations may be used to qualify the aggressiveness of leading edge cavitation and that the concept of the Cavitation Erosion Power is a good basis to scale cavitation damage. Furthermore, the envelope of the vibrations signals is found to be coherent with transient pressure signals.

NOMENCLATURE

A	Power density spectrum of the acceleration signal	[dB re 1 g^2/Hz]
$\hat{A}$	Power density spectrum of the acceleration envelope	[dB re 1 g^2/Hz]
L	Chord length of the hydrofoil	[m]
E_c	Potential energy of a single cavity	[J]
$\dot{E}_c$	Cavitation Erosion Power	[W]
P_i	Power density spectrum of the pressure p_i	[dB re 1 Pa^2/Hz]
Re	Reynolds number $= \frac{UL}{\nu}$	[-]
St	Strouhal number $= \frac{f\,l}{U}$	[-]
U	Upstream velocity	[m/s]
V_c	Traveling cavity volume	[m^3]
a	Acceleration signal	[ms^{-2}]
$\hat{a}$	Envelope of the acceleration signal	[ms^{-2}]
c_p	Pressure coefficient $= \frac{p-p_{ref}}{\frac{1}{2}\rho U^2}$	[-]
c_{pc}	Pressure coefficient at the cavity closure	[-]
f	Frequency of the main cavity pulsation	[Hz]
h	Main cavity height	[m]
i	Incidence angle of the hydrofoil	[°]
l	Main cavity length	[m]
p_i	Pressure measured by the transducer #i	[Pa]
p_c	Pressure at the cavity closure	[Pa]
p_{ref}	Reference pressure at the test section inlet	[Pa]
p_v	Vapor pressure	[Pa]
ρ	Water density	[kg/m^3]
σ	Cavitation index $= \frac{p_{ref}-p_v}{\frac{1}{2}\rho U^2}$	[-]
ν	kinematic viscosity of the water	[m^2/s^2]
K	A constant	

Abbreviation

PSD	Power Density Spectrum

INTRODUCTION

Although the problem of cavitation erosion has received a great deal of attention, one is still unable today to predict the intensity and the rate of the cavitation erosion in hydraulic machines with an acceptable accuracy. Nevertheless, important progress has been achieved in understanding the mechanisms of the erosion process. Many authors agree that the leading edge cavitation in hydraulic machines is one of the most dangerous situations from the erosion point of view. In fact, the vorticity generation on the fixed cavity leads to the formation of swirling cavities. These U-shaped cavities, also called cloud cavitation, are convected by the mean flow to the pressure recovery region where they collapse. We have investigated (Avellan et al, 1989) a single cavitation vortex dynamics and have shown that vortex collapse leads to a strong shock wave generation with a resulting over pressure that may reach up to 2 GPa. Dupont (1991) studied the leading edge cavity dynamics with the help of flow field velocity measurements. He demonstrated that vorticity lines are generated early on the main cavity surface due to intense shear stress in the vapor-liquid interface. The interaction of these vorticity lines with the Kelvin-Helmholtz instabilities leads to the U-shaped vortices formation similar to those observed downstream a bubble separation by Sasaki et al (1992). Franc (1985) investigated the interaction between the main cavity and the boundary layer and pointed out the influence of the incidence angle on the leading edge cavitation behavior. Simoneau (1989) and Bourdon (1990) performed on line cavitation erosion measurements in the IMHEF high speed cavitation tunnel.

We have introduced in a previous work (Avellan et al, 1992) the model of Cavitation Erosion Power based on the assumption that severe erosion is usually due to the repeated collapses of transient vortices shed by a main cavity attached to the leading edge of the blade. We also assumed that the intensity of a single collapse is related to the potential energy E_c of the traveling cavity corresponding to its maximum volume V_c:

$$E_c = (p_{max} - p_v)\, V_c$$

Where p_v is the vapor pressure and p_{max} is the maximum pressure responsible for the cavity implosion.

Assuming that the traveling cavity dimensions may be scaled by the main cavity length, we have shown that cavitation erosion intensity may be scaled by a simple set of flow parameters depending on the mean upstream velocity U, the Strouhal number St corresponding to the main cavity fluctuations and the cavity length l. The Cavitation Erosion Power $\dot{E}_c$ may be written as follows :

$$\dot{E}_c = \frac{1}{2} K \rho (C_{p_{max}} + \sigma)\, St\, U^3 l^2$$

In the present work, we intend to validate the concept of Cavitation Erosion Power by achieving synchronous measurements of the pressure fluctuations downstream of the leading edge cavity and the main cavity dimensions. We will show how the pressure fluctuations may be taken as a representative parameter to relate the cavitation erosion aggressiveness. The pressure fluctuations levels are then compared to the cavitation erosion power. Furthermore, simultaneous measurements of the cavitation induced vibrations are achieved. We will show how the vibrations signals may be processed to extract meaningful information about the cavitation erosion process. Furthermore, pressure fluctuations and vibrations measurements in conjunction with the flow visualization allow a deeper analysis of the erosive cavities dynamics.

Pressure fluctuations are measured with the help of transient pressure transducers mounted on the suction side of a 2D hydrofoil. The vibrations are measured by an accelerometer attached to the blade. The cavity dimensions are measured by an optical technique using a laser sheet as reported by Kueny (1991).

EXPERIMENTAL SET-UP

The tests are carried out in the IMHEF high speed cavitation tunnel (Avellan et al., 1987) with a 150x150x750mm test section where a maximum velocity of 50 m/s may be achieved.

Pressure Instrumentation

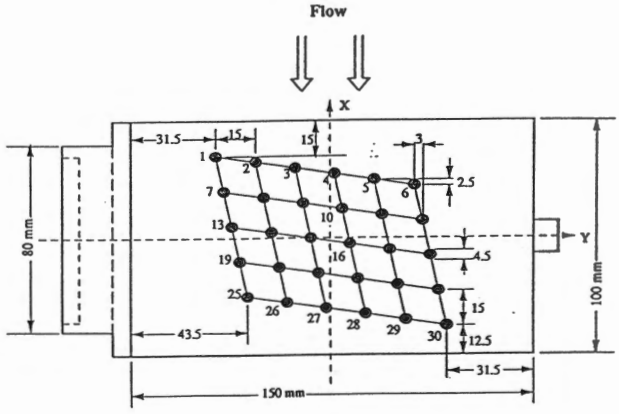

Figure 1 : NACA009 hydrofoil equipped with 30 transient pressure transducers

The experimental hydrofoil is a 2D NACA009, 100 mm long and 150 mm wide, truncated at 90 % of its length. 30 piezoresistive absolute pressure transducers are distributed on the suction side of the blade, Figures 1 and 2. The measurement range covers 0 to 200 bar. Each transducer is supplied by an independent current source and its output pressure signal is separately amplified and band-pass filtered. Data acquisition is performed with the help of two digital transient recorders with a 12 bits resolution per sample. The first one allows simultaneous data acquisition of 32 signals at a maximum sampling frequency

of 5 kHz whereas the second one ensures simultaneous data acquisition of 12 channels at a maximum sampling rate of 1 MHz.

Pressure calibration

Static calibration of the pressure transducers is performed with the blade mounted in the test section by varying the static pressure in the tunnel from 0.1 to 10 bar.

To achieve a dynamic calibration of the pressure transducers, a special technique is developed to generate a pressure impulse in the test section. A discharge of 5 to 50 Joule electric energy is performed through coaxial probes previously introduced in the test section. The use of a high speed electronic switch allows a discharge duration ranging from 5 to 20 µs. An explosive growth of a vapor bubble takes place in the test section leading to a strong pressure impulse generation used to excite the pressure transducers in a wide frequency band (from 100 Hz to 100 kHz). Transducers outputs are then compared to the output of a 601 Kistler pressure transducer flush mounted to the test section. Transfer functions are averaged over 32 shots.

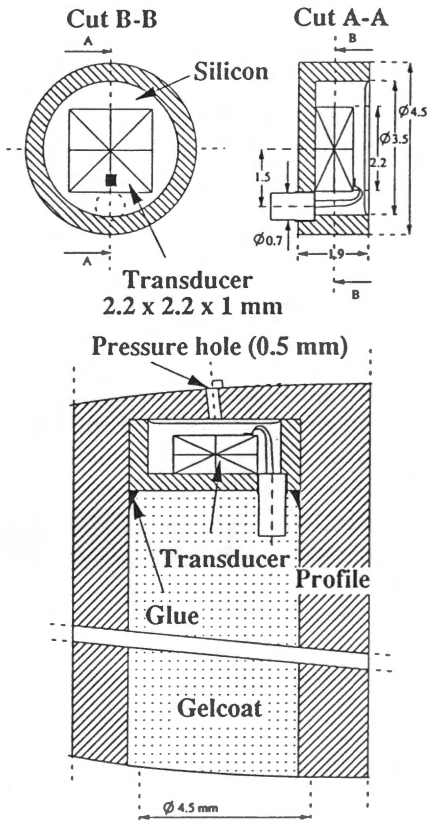

Figure 2: Pressure transducer mounting

Vibrations measurements

Measurements of cavitation-induced vibrations are carried out with the help of a 8309 Brüel&Kjær accelerometer with 175 kHz natural frequency. This transducer is mounted on the blade housing 100 mm apart from the test section wall.

Transient calibration of the accelerometer is performed by hitting the blade with an instrumented hammer. The resulting force impulse has a typical duration of 20 µs. The response of the accelerometer is compared to the output of the hammer built-in force transducer.

Visualization

A CCD camera is used to capture the shape of the leading edge cavity with a laser light sheet illumination, see Figure 3. The light sheet is generated by focusing a 5 Watt argon laser beam on a cylindrical lens; very short light pulses down to 2 µs are achieved with an electro-optical shutter. Image acquisition is performed with a video frame grabber; the video signal is digitized with a rate of 25 frames per second into 300x50 pixels image with a resolution of 8 bits.

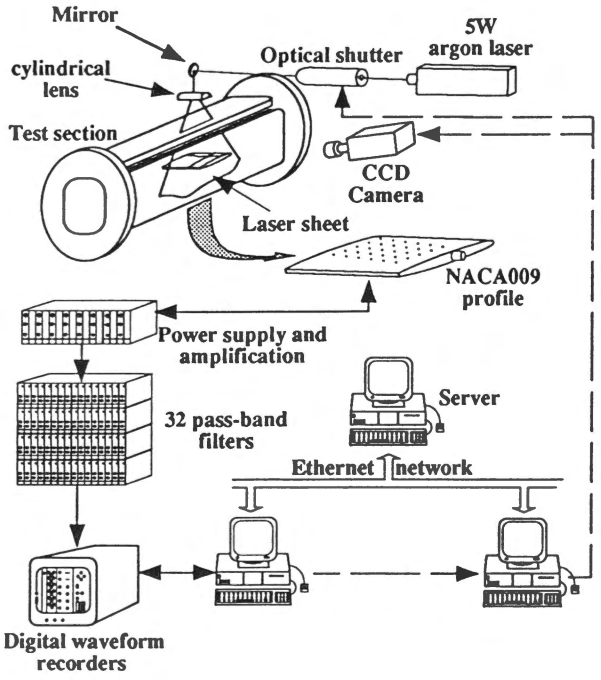

Figure 3: Experimental setup

The subsequent image processing is performed in order to determine the length l and the maximum thickness h of the leading edge cavity. First, gray level weighting of the cavity outline is achieved. The resulting curve is then fitted by a least square

polynomial approximation. Figure 4 shows an example of the main cavity outline for upstream velocities of 30 and 32m/s and incidence angles of 2.5° and 3°.

Furthermore, high speed visualization of the cavitation flow is performed with the help of a rotating drum camera with a maximum rate of 200,000 frames per second.

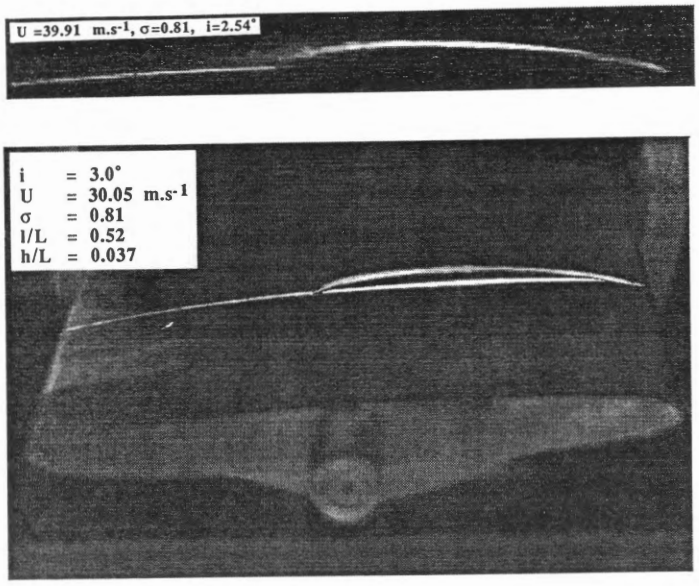

Fig. 4: Visualizations of the leading edge cavity with the laser light sheet

RESULTS AND DISCUSSIONS

Main cavity dynamics

The behavior of the leading edge cavity was observed for upstream velocity, incidence angle and cavitation index being varied in a wide range. Figures 5 and 6 show two examples of the leading edge cavitation development for 30 m/s upstream velocity and incidence angle of 2.5° and 3.5°. We have plotted on the same figures the corresponding time history pressure signals in the cavity closure.

We can observe that the cavity detachment is made of spots that grow in width downstream. It was observed that an increase of the Reynolds number as well as an increase of the incidence angle, lead to an increase of the number of these cavitation spots and a decrease of their width.

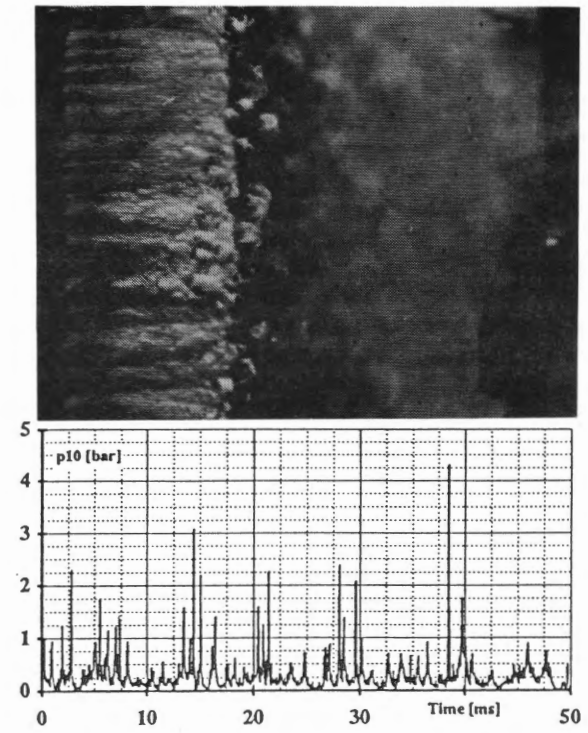

Figure 5: visualization of leading edge cavitation with the corresponding time history pressure in the cavity closure for U = 30 m/s, i = 2.5°, σ = 0.75

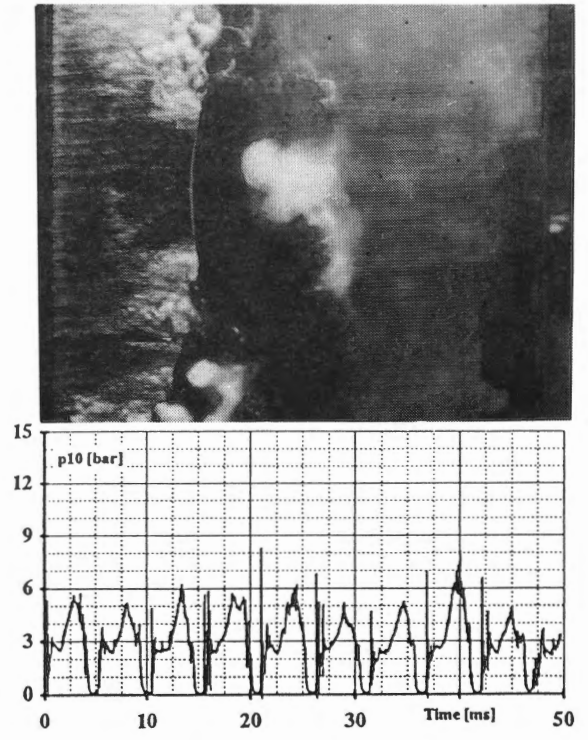

Figure 6: visualization of leading edge cavitation with the corresponding time history pressure in the cavity closure for U = 30 m/s, i = 3.5°, σ = 0.98

For a given cavity length and upstream velocity, the main cavity behavior is very sensitive to the incidence angle as shown on Figures 5 and 6. The range of behavior can be classified into two main types. Firstly, when incidence angle is low (< 3°), the main cavity is stable and the generated vortices have a small size in comparison to the cavity length. In the second case which occurs when the incidence angle is increased, the main cavity becomes unstable with the induced noise and vibrations being drastically increased. In this case, the size of transient vortices is similar to the cavity length and one may easily observe the re-entrant jet that many authors have already reported. The broad band pressure signals show a deep difference between these two regimes, Figure 5 and 6.

A significant influence of the Reynolds number on the main cavity dynamics has been also observed : as already reported by Dupont (1992), an increase of the Reynolds number leads to a slight increase of the main cavity length for a fixed cavitation index. Furthermore, the incidence threshold leading to unstable cavity behavior decreases when the upstream velocity is increased: For a cavity length l=0.4L, this incidence threshold drops from 2.5° to 2° when the upstream velocity is varied from 15 m/s to 35m/s.

Furthermore, it was also observed that increasing the cavity length leads to a decrease of the incidence threshold corresponding to transition to unstable behavior.

The fundamental mechanisms of unsteady cavitation is not fully understood. A plausible explanation would be that the incidence angle as well as the Reynolds number act on the main cavity behavior through the boundary layer change that they cause. When the incidence angle or the Reynolds number are increased, it was observed that the detachment point as well as the transition point from transparent to wavy aspect of the main cavity move toward the leading edge. This suggests that the change of the cavity aspect from transparent to wavy may be due to the transition to turbulence in the liquid flow as reported by Franc (1985). Thereby, the unstable behavior of the main cavity may be explained by the fact that the transition to turbulence reaches the detachment point. A large part of the main cavity is then periodically swept and reconstructed with large scale vortices being generated. The resulting fluctuations of the lift component explains the sudden increase of the vibrations and noise levels.

Unsteady cavitation may also result from a lock-in between the main cavity pulsation and the transient vortices generation that happens when the frequencies of these two different processes become close to each other.

From erosion point of view, the unsteady cavitation is of major interest: In fact, Owing the erosion rate measurements performed by Simoneau (1989) and Bourdon (1990), cavitation severity increases drastically when unsteady cavitation takes place.

The main cavity dimensions are measured for upstream velocity varying from 20 m/s to 40 m/s and for incidence angles of 2.5°, 3.0°, 3.5°, and 4.0°. Figure 7 shows the evolution of the main cavity height h, versus its length l both normalized by the chord length L. This curve reveals a linear relationship between the length and the height of the main cavity. The ratio h/l depends slightly on the incidence angle and was found to lie between 7 and 8 %. Nevertheless, data dispersion may be observed for high incidence angles (i>3°). In fact, accuracy of measurements of the cavity dimensions drops when the unstable regime takes place because of the high amplitude oscillation.

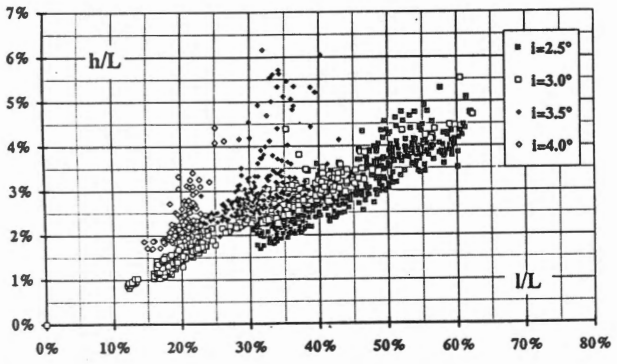

Figure 7: Cavity height vs cavity length

Figure 8 shows the variation of the main cavity length with the cavitation index σ for different upstream velocities and incidence angles.

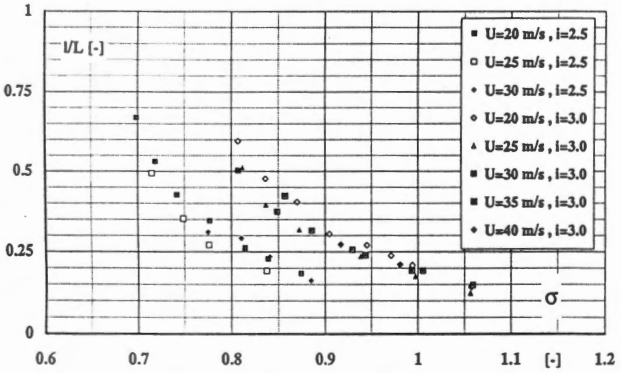

Figure 8: Cavity dimensions vs the cavitation index

Figure 9 shows the distribution of mean values and rms values of the wall pressure along the blade for upstream velocity of 19.96 m/s, incidence angle of 3 ° and a cavitation index of 0.87. We have presented on the same figure the main cavity outline. Averages and rms estimation are performed over 16 batches of 1,024 samples each recorded at 5 kHz sampling frequency.

It should be noticed that the maximum pressure fluctuations occurs directly downstream the main cavity. Simoneau (1990) measured the erosion rate on the same hydrofoil and found that

the maximum of erosion occurs in this same area. Therefore, we can state that the pressure fluctuations are representative of the cavitation aggressiveness.

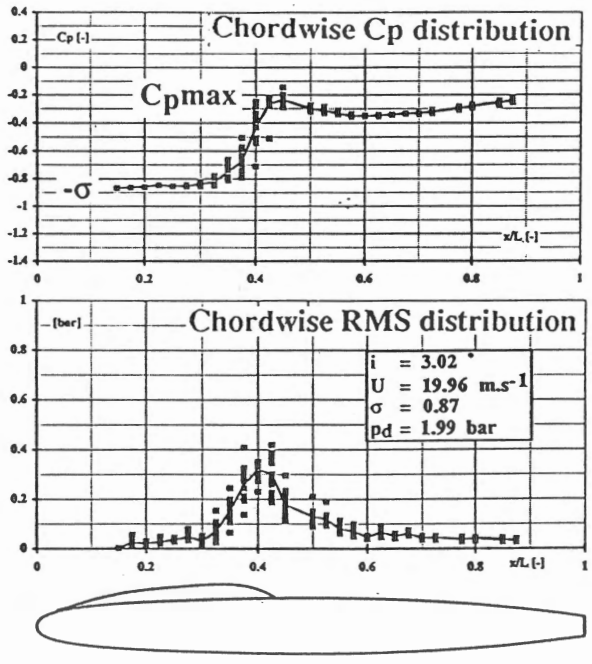

Fig. 9: Mean and rms values of the pressure with the main cavity outline captured by the laser light sheet.

The dynamics of transient cavities

Spectral analysis of the pressure fluctuations is performed by averaging power density spectra with an overlap coefficient of 50%, over 16 contiguous batches of 8,192 samples each. Time history signals are high-pass filtered to 20 kHz and digitized at 200 kHz sampling frequency.

We have presented in Figure 10 power density spectra at the cavity closure for an incidence angle of 3° and an upstream velocity varying from 20 m/s to 36 m/s. These spectra show that most of the pressure fluctuations energy is concentrated around a main frequency which grows with the upstream velocity. Since the corresponding transducer is located at the cavity closure, this frequency corresponds obviously to the main cavity pulsation.

The power density spectra shown on Figure 11 correspond to the pressure signals p_4, p_{10} and p_{16} recorded simultaneously. The upstream velocity is 28.0 m/s and the incidence angle is 4°. The cavitation index is set to 1.34 leading to the pressure transducer #4 being at the main cavity closure.

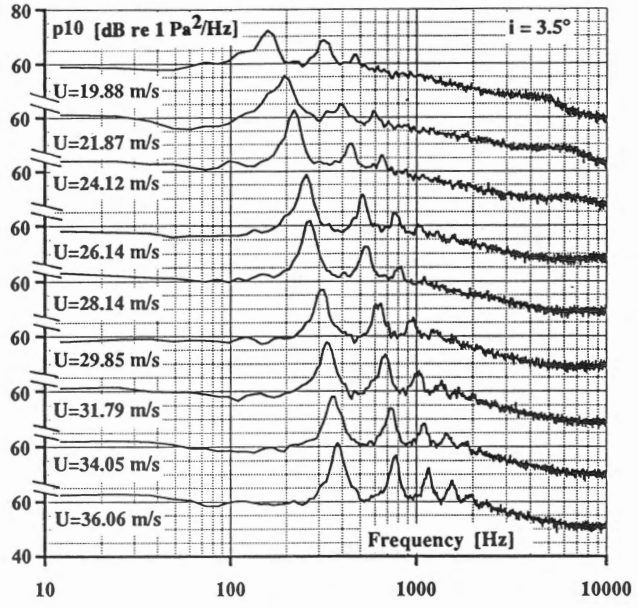

Fig. 10: Power density spectra of the pressure p_{10} for different upstream velocities

The same main frequency is observed on the three spectra. For p_{10} and p_{16}, this main frequency corresponds obviously to the transient cavities passage since the transducers #10 and #16 are far enough from the cavity closure. The coherence functions plotted on the same Figure, show a good linearity between any pair of pressure signals in a narrow frequency band around the shedding frequency. The poor coherence observed outside this interval reveals a total independence between pressure fluctuations. In this case (i=3.5°), the transient cavities generation is strongly modulated by the main cavity pulsation.

The influence of the incidence angle is shown, Figure 12. Power density spectra of the pressure are plotted for incidence angles of 2.5°, 3°, 3.5° and 4°. The upstream velocity is fixed to 25 m/s and the cavity length is 22 mm.

The main frequency observed on the pressure spectrum for incidence angles higher than 3° is no longer visible when the incidence angle is reduced (i<3°). This is due to the deep change of the leading edge cavity behavior as we have previously described in this paper. Thereby, we can state that the shedding process of the transient cavities doesn't show any main frequency while it becomes almost periodic when the unstable cavitation regime takes place.

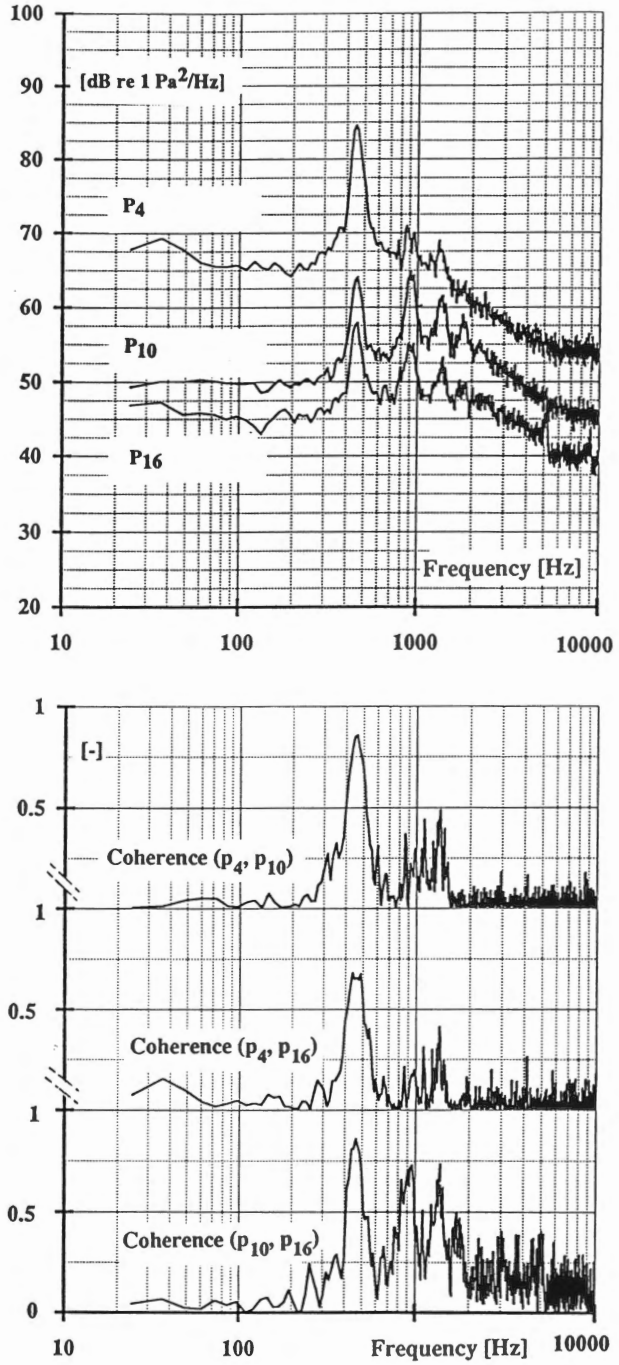

Fig. 11: Power density spectra and coherence functions for pressure signals p_4, p_{10} and p_{16}

We have plotted on Figure 13 the frequency of transient cavities generation as a function of the ratio U/l for incidence angle taken as 3°, 3.5° and 4°

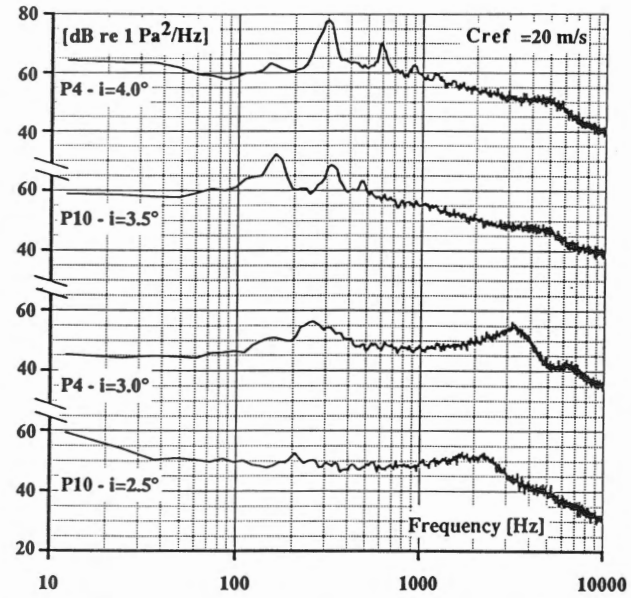

Fig. 12 : Influence of incidence angle on pressure fluctuations

We can observe that for a given incidence angle, the Strouhal number St remains almost constant when the cavity length or the upstream velocity are varied. the following table gives the averaged Strouhal number for each incidence angle tested :

Incidence angle	Strouhal Number
3.0°	0.23
3.5°	0.29
4.0°	0.32

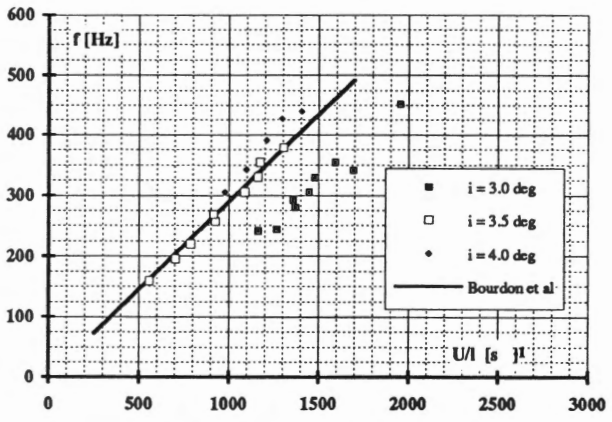

Fig. 13 : Shedding frequency vs. the ratio $\frac{U}{l}$

The low value of the Strouhal number in the case of 3° incidence angle may be due to an uncertainty on the main frequency measurement since this incidence corresponds to the transition to unsteady behavior which is characterized by strong intermittence.

Vibrations

First, let us examine the influence of the blade vibrations induced by the Karman vortices generated at the trailing edge. Figure 14 shows the power density spectra corresponding to pressure p_{10} as well as the acceleration signal. The upstream velocity is 15 m/s, the incidence angle is 3° and the sigma value is set in such a way that the main cavity closure is located on the pressure transducer #4. These spectra show peaks at the same frequency of 860 Hz which corresponds to an eigen frequency of the blade. In this case, the Strouhal number is 1.75 which is far from the value of 0.23 already found for the same incidence angle outside the lock-in regime. Thereby, the blade vibrations forces the cavity to pulsate at the blade eigen frequency and the Strouhal law is no longer available. Nevertheless, when the main cavity length is increased (l>0.4L), this forced regime of the cavity fluctuations is no longer observable. This is obviously due to the cavitation induced disturbances on the Karman vortices.

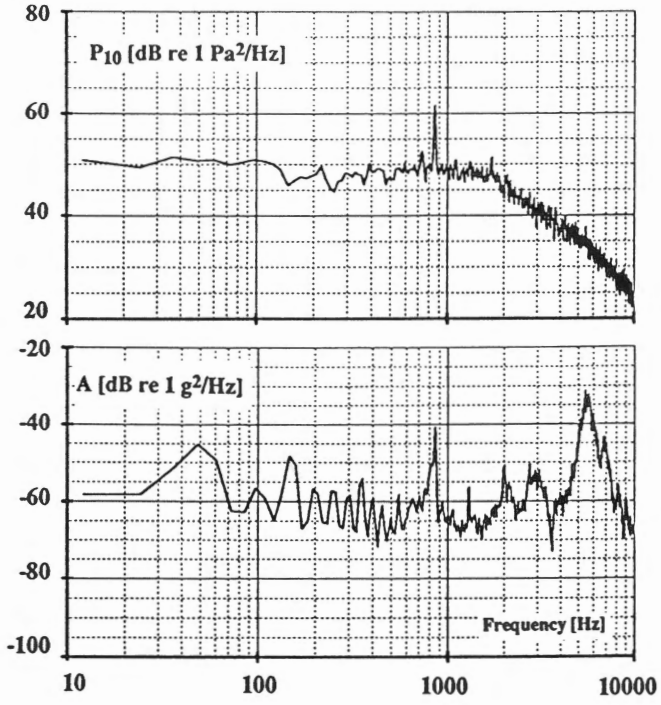

Fig. 14: Pressure and vibrations power density spectra in the case of resonating blade du to Karman vortices

This result is interesting for two main reasons : first, it shows that the shedding process may be controlled by external actuators which may be performed by hydrophones. Secondly, it explains why in hydraulic machines the shedding process is always modulated by the blade passage frequency or the wicket gate frequency as observed by Bourdon et al (1993) and Abott (1989).

Figure 15 shows power density spectra corresponding to the pressure p_{10} and the acceleration signal both simultaneously recorded. The upstream velocity is 28 m/s, the cavitation index is 1.1 and the incidence angle is 4° which leads to unsteady cavitation regime. The Strouhal frequency which is well observed in pressure spectrum is hardly visible in the acceleration spectrum. This is confirmed by a poor coherence, Figure 15. In fact, the pressure pulses resulting from the collapses of traveling cavities excites the solid structure in a wide frequency band. Therefore, the accelerometer is rather sensitive to eigen frequencies of the structure and Fourier transform processing is not suitable.

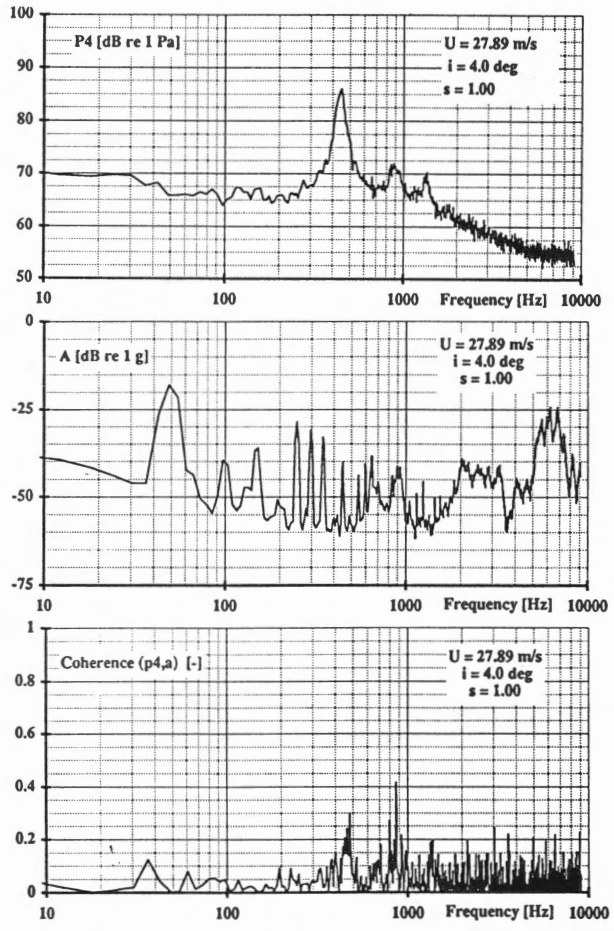

Fig. 15: Pressure and vibrations spectra with their corresponding coherence function.

Further processing is then performed on vibrations signals. The signal envelope in the frequency band [1, 5 kHz] is derived from the Hilbert transform using digital band pass filter. Figure 16

illustrates the envelope spectrum corresponding to the acceleration signal of Figure 14. The shedding frequency is now well observed on the acceleration envelope. The coherence function plotted on the same Figure shows a good linearity between the acceleration envelope and the pressure signals.

It should be noticed that the choice of the frequency band used to perform envelope calculation is important. This interval, that has to be as narrow as possible, should contain only frequencies concerned by the collapse of the traveling cavities. Energy corresponding to frequencies outside the useful band is related to other noise sources such as the tunnel pump and doesn't contain meaningful information on the cavitation erosion process. In our case, the useful frequency band is derived from the frequency response of the accelerometer by selecting the most energetic part of the transfer function.

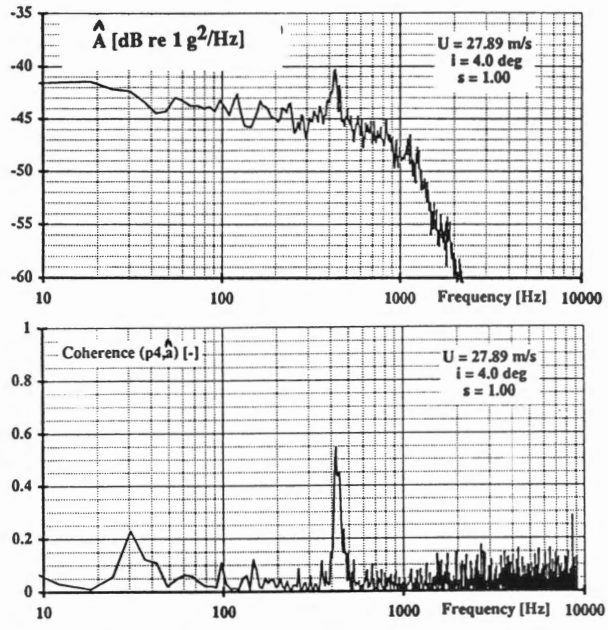

Fig. 16 : Acceleration envelope PSD and coherence function with the transient pressure

Cavitation erosion power

For a given set of hydrodynamic conditions, as soon as we can estimate the vortex shedding frequency, we may calculate the cavitation erosion power, as defined in the introduction. Therefore, only unstable cavitation (i>3°) is considered to validate the concept of the erosion power. This restriction is for low consequences since lock-in conditions are known to be much more dangerous from the erosion point of view.

We have plotted on Figure 17 the power density spectra scaled by the cavitation erosion power as a function of the term fl/U for an incidence angle of 4° and a cavitation index of 1.2. The velocity is varied from 20 to 28 m/s. These spectra collapse to almost one curve with a maximum of energy being concentrated around the Strouhal frequency. It should be noticed that even if a poor coherence is observed for the frequencies standing outside a narrow interval around the Strouhal frequency, the pressure spectra are well scaled by the erosion power in the whole frequency band [0, 10 kHz].

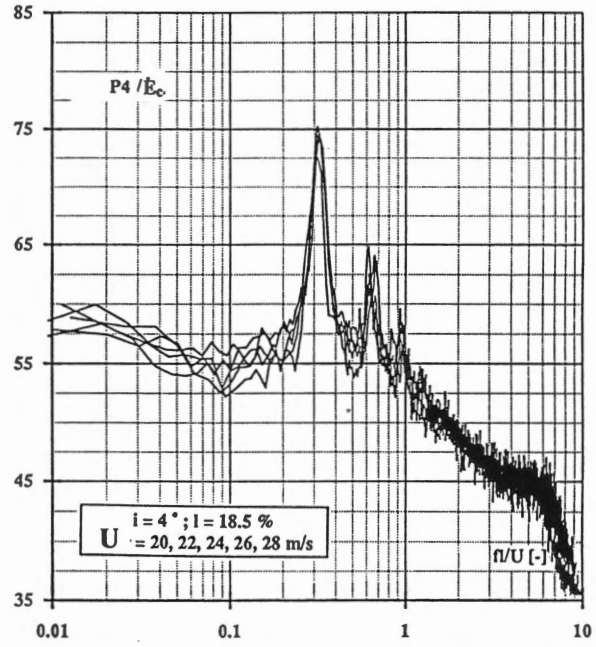

Fig. 17 : p_{10} power density spectra scaled by the cavitation erosion power vs $\frac{f\,l}{U}$

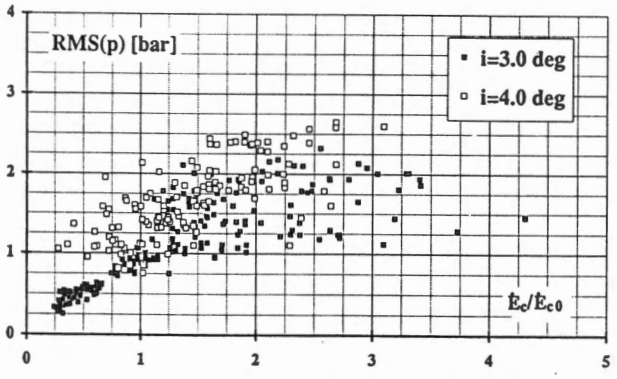

Fig. 18 : rms values of the pressure fluctuations vs the cavitation erosion power.

The rms values of the pressure fluctuations in the frequency band [0, 25 kHz] are plotted Figure 18 as a function of the cavitation erosion power $\dot{E}_c$ normalized by an arbitrary value $\dot{E}_{c0}$

corresponding to an upstream velocity of 20 m/s, an incidence angle of 4° and a cavity length of 20 mm. These data correspond to a wide range of variation of hydrodynamic conditions.

A roughly linear relationship is observed between rms values of the pressure fluctuations and the Cavitation Erosion Power. However, some dispersion is visible; this was somehow expected because of our simple assumption that the volume of traveling cavities may be scaled by the main cavity length. In fact, we have shown that for a given main cavity length, the size of traveling vortices is very sensitive to the incidence angle. Thereby, in order to improve the model of Cavitation Erosion Power, the relationship that links the volume of traveling cavities with hydrodynamic conditions has to be investigated.

CONCLUSIONS

Pressure fluctuations downstream of a leading edge cavity have been measured with simultaneous measurements of the main cavity dimensions and the cavitation-induced vibrations. Conclusions may be summarized as follows :

1. Leading edge cavitation is very sensitive to the incidence angle. It was demonstrated that beyond an incidence threshold which depends on the cavity length and the Reynolds number, unsteady cavitation takes place leading to large vortex generation and high level induced noise and vibrations. besides the interaction with the boundary layer, another reason of this unsteadiness may be due to a lock-in between the main cavity pulsation and the transient vortices generation.

2. The main cavity length and height vary in a linear way. The ratio h/l is slightly sensitive to the incidence angle and lies between 7% and 8%.

3. The maximum of the pressure fluctuations occurs in the vicinity of the main cavity closure. This result confirms the fact that pressure fluctuations are representative of the cavitation aggressiveness in leading edge cavitation flow.

4. In the case of steady cavitation, no main frequency could be detected for the shedding process. In contrast, unstable regime leads to the generation process being periodic and strongly modulated by the cavity pulsation. In this case, the shedding process follows a Strouhal like law. Furthermore, the blade resonance induced by the Karman vortices forces the cavity to pulsate at the blade resonance frequency. In this particular case, the transient vortices generation is modulated by the main cavity pulsation and the Strouhal law is no longer available.

5. When the cavity is unstable, the envelope of the acceleration signal in a well chosen frequency band has its maximum energy around the Strouhal frequency.

6. The rms values of the pressure fluctuations varies approximately in a linear way with the cavitation erosion power leading us to believe that it stands as a good basis for prediction of the cavitation erosion in hydraulic machines. Nevertheless, further work has to be achieved to improve the model of cavitation erosion power. Namely, direct measurements of the volume of traveling vortices needs to be performed.

ACKNOWLEDGMENTS

The present work would not have been possible without the help of the members of the IMHEF cavitation Research Group. Authors would like to thank Dr. Bourdon P. for his interesting comments about digital data analysis. This research program is financially supported by the Swiss Federal "Commission d'Encouragement à la Recherche Scientifique", the Swiss Energy Producers Association "National Energie Forschung Fonds", Sulzer Brothers and Hydro Vevey.

REFERENCES

[1] **Abbot, P.A**, "Cavitation Detection measurements on Francis and Kaplan Hydroturbines", Proceedings of International Symposium on Cavitation noise and Erosion in Fluid Systems, ASME Winter annual meeting, San Francisco (USA), Dec 1989.

[2] **Avellan, F., Dupont, Ph., Farhat, M.**, "Cavitation Erosion Power", Proceedings of the First ASME-JSME Fluids Engineering Conference, Portland, Oregon, USA, 23-27 June 1991, FED-Vol. 116, pp. 135 - 140.

[3] **Avellan, F., Henry, P. and Ryhming, I.L,** "A New High Speed Cavitation Tunnel", ASME Winter Ann. meeting,1987, FED Vol. 57.

[4] **Avellan, F., Farhat, M.** , "Shock Pressure Generated by cavitation vortex collapse", Proceedings of International Symposium on Cavitation noise and Erosion in Fluid System, ASME Winter annual meeting, San Francisco (USA), FED-Vol. 88, Dec 1989, pp 119-125.

[5] **Bourdon, P., Simoneau, R., Avellan, F.**, "Hydraulic Turbine Cavitation Pitting Detection by Monitoring runner vibration", Final Research Report 307G657, submitted to the Canadian Electrical Association, Juin 1993.

[6] **Bourdon P., Simoneau R., Avellan F., Farhat M.,** " Vibratory characteristics of erosive cavitation vortices downstream of a fixed leading edge cavity ", Proceedings of IAHR 15th Symposium, Belgrade, Yugoslavia, 11-14 September 1990, Vol. I, paper H3, 12 pages.

[7] **Dupont Ph.**"Etude de la dynamique d'une poche de cavitation partielle en vue de la prediction de l'erosion dans les turbomachines hydrauliques", PHD thesis, EPFL Lausanne, 1992.

[8] **Franc J. P.**"Attached cavitation and the boundary layer: experimental investigation and numerical treatment", J. Fluid Mech., 1985, vol. 154, pp 63-90.

[9] **Kueny J. L., Rebou J. L** "Analysis of Partial Cavitation: Image Processing and Numerical Prediction". Proceedings of the First ASME-JSME Fluids Engineering Conference, Portland, Oregon, USA, 23-27 June 1991, FED-Vol. 116, pp. 55-60.

[10] **Simoneau, R., Avellan, F., Kuhn de Chizelle, Y**, "On line measurement of cavitation erosion rate on a 2D NACA profile", Proc. of International Symposium on Cavitation noise and Erosion in Fluid Systems, ASME meeting, San Francisco (USA), FED-Vol. 88, Dec 1989, pp 95-102.

[11] **Sasaki, K., Kiya, M.**, "Three-dimentional Vortex Structure in a leading edge Separation bubble at moderate Reynolds Numbers", Journal of Fluid Dynamics, September 1992, Vol. 113, pp 405-410.